JOURNAL OF AIRCRAFT
Vol. 44, No. 5, September–October 2007

Steep-Descent Maneuver of Transport Aircraft

Antonio Filippone*
University of Manchester, Manchester, M60 1QD England, United Kingdom

DOI: 10.2514/1.28980

This paper solves the problem of steep descent of jet-powered transport aircraft. The cases considered involve a continuous descent approach. Steep descent is interpreted as a flight path with glide slope up to 5.5 deg. Several requirements are discussed in detail; these include safety limits, stall control, and noise emission. First, parametric analysis of the aerodynamic coefficients are shown to indicate where existing aerodynamic data would fail to achieve a steep descent. Second, flight trajectories are calculated as a two-value boundary value with constraints on the terminal descent rate, on the air speed, and the lift coefficient. The effects of landing weight, starting altitude, and a relax on the terminal constraint are simulated. Third, parametric changes in the aerodynamic polar and drag are proposed to accommodate changes required in the flight controls. Fourth, a noise model of the aircraft is presented, and calculations are performed at the reference flight paths to verify whether the overall sound pressure level at a reference point (FAR Part 36) is below the noise at the nominal flight path. The aircraft simulated is the Airbus A-310-200 with CF6-80C2 engines. It is concluded that 1) the highest descent angle for this aircraft is about 4–4.5 deg; 2) a steeper descent can be achieved with an increase in both the maximum lift and the zero-lift drag, with the condition that $C_D/C_L^{3/2}$ also increases; 3) noise is reduced by up to 6.0 dB, mostly due to the larger distance from the receiver; and 4) the maneuver time is reduced by up to 60 s.

Nomenclature

A	=	wing area
a	=	parameter defined by Eq. (6)
b	=	wing span
C_D	=	drag coefficient
C_{D_o}	=	zero-lift drag coefficient
C_L	=	lift coefficient
$C_{L_{\max}}$	=	maximum lift coefficient
c	=	wing chord; constant factor
c_i	=	constant coefficients ($i = 0, 1, 2, \cdots$)
D	=	drag force
f_d	=	$C_D/C_L^{3/2}$
f_j	=	the same as thrust-specific fuel consumption
g	=	acceleration of gravity
h	=	altitude
k	=	lift-induced drag factor
k_i	=	lift-induced drag factors ($i = 1, 2$), Eq. (20)
k_s	=	stall margin, Eq. (14)
L	=	lift force
m	=	mass
P, P_1, P_2	=	aerodynamic factors, Eq. (21)
q	=	dynamic pressure
r	=	distance noise source to receiver
T	=	engine thrust; net thrust
T_{av}	=	available thrust
t	=	time
V	=	air speed
v_s	=	descent rate
W	=	weight
X	=	flight distance
x	=	nondimensional quantity, Eq. (18)
γ	=	descent angle
δ_f	=	flap deflection
Λ	=	wing's sweep angle
Π	=	throttle setting
ρ	=	air density
σ	=	relative air density

Subscripts

a	=	air
f	=	fuel quantity
j	=	relative to a jet, or jet engine
o	=	sea level, standard, stagnation, or initial conditions
p	=	parasite
qc	=	quarter-chord
r	=	reference quantity
to	=	value at takeoff
tp	=	tailplane
w	=	wing

Superscripts

$-$	=	mean value
$\cdot$	=	time derivative

Received 22 November 2006; revision received 22 December 2006; accepted for publication 25 December 2006.

*School of Mechanical, Aerospace and Civil Engineering, George Begg Building, P.O. Box 88; a.filippone@manchester.ac.uk. Senior Member AIAA.

I. Introduction

TRANSPORT aircraft have glide slopes on approach around 2.5–3 degrees. One of the consequences of this maneuver is to expose large populated areas to noise emission. An aircraft descending at 3 deg from 1500 ft (457 m) would cover 7 n miles before landing. Shallow descent flight paths also increase the time between landings at busy airports. If a steeper approach could be achieved without noise penalty and without compromising the flight safety, then the aircraft could land at airports with limited access (airports at the edge of hills, large bodies of water, industrial estates) and with considerable built-up areas around the airfield. In recent years, a number of smaller airports have been opened up to commercial traffic in Europe. These include municipal airports for general aviation and converted military airports. Most of these airports are within city boundaries, and have constraints on both noise and accessibility.

London City airport has set the glide slope at 5.5 deg. This constraint raises concerns with airlines. Smaller airplanes, such as the BAe Systems RJ 146, already operate at this airport. The Embraer 170 uses air brakes to increase its descent rate. Clam shells mounted at the rear part of the fuselage are used to increase the drag, and hence

the descent rate. These shells can also function on the runway in lieu of reverse thrust.

The Airbus A-318 has recently run a test flight into London City. Embraer need special certification to operate the -190 model at such a steep glide path. The combination of these needs and constraints requires a rational solution to the terminal maneuver area (TMA) of commercial aircraft. This problem is the subject of the present investigation.

The steep descent has been discussed recently by Antoine and Kroo [1], who estimated the noise reduction of a steep approach (4.5 deg) by as much as 7.7 dB, although this result was obtained with a conceptual design of a heavier aircraft. The analysis required, among other things, to operate at a reduced throttle (thrust), which in turns contributes to the reduction of engine noise (in particular, fan noise). However, this estimate is optimistic, because a steeper approach with a higher drag may require to *increase* the throttle, instead of decreasing it. Also, if the throttle were to remain at the same level as the nominal approach path, the aircraft would slow down as a consequence of increased drag, with a risk of stalling. The Federal Aviation Regulations (FAR) have specific requirements on the approach speed and the stall speed. Hence, the reduction of air speed must be carefully considered. Past experience shows that there is an evident correlation between accidents and approach speed.

The conventional approach is a segment descent, with the aircraft descending to 2000 ft, then following a level path. The final segment consists of a rectilinear path along the extended runway center. Because of the complexity of management of the air space, airplanes are generally instructed by the Air Traffic Control (ATC) to follow specified patterns at fixed altitudes and speeds, so as to predict their position and heading at all times.

Each airport has its own geographical constraints. In some cases the aircraft is forced to make a sharp turn before the final approach. These cases include prevailing winds and obstacle avoidance. In recent years new descent procedures have been developed, such as the continuous descent approach (CDA). This is a procedure in which the aircraft descends continuously from a relatively high altitude to minimize landing time, engine emissions, and community noise. In broad terms, the CDA is a flight path in which the aircraft joins the final instrument landing system (ILS) glide path at an appropriate altitude for the distance from the runway, without recurring to a level flight. The point at which the ILS glide slope is joined can be higher than the conventional flight path.

An example of this maneuver is given by Amsterdam Schipol [2,3]. An advanced continuous descent approach (ACDA) at this airport involves a 180-deg turn with a 2 n mile turn radius starting from flight level FL70, before approaching the ILS glide slope extending from the center of the runway. Comparisons of aircraft performance between the conventional landing of a Boeing B-747-300 and the CDA show that the engine and the fan run at lower rpm; thus, they contribute to the reduction of the engine noise. However, it has been found that the maneuver involves a doubling of the landing time, from 2 to 4 min. An increase in flight time has been calculated by other investigators, and that seems to be a major concern at airports with high traffic.

The CDA has been further developed by Clarke et al. [4] and tested at Louisville International Airport. A Boeing B-767-300 showed peak noise reduction variable between 3.9 and 6.5 dBA, and a fuel reduction up to 227 kg. These authors used an aircraft noise program along with a flight simulator for the Boeing B-757 and B-767.

Another aspect of CDA is the additional control required. This has limited its application to places with relatively low volume of traffic. However, the procedure has been developed by Boeing [5] for landing on two parallel runways at Houston Intercontinental.

Several options have been proposed for tackling aircraft noise. These include night-time curfews, phasing out of older airplanes, new engine technology, and even acoustic insulation of houses at the expense of the airports. However, the most effective option remains the operation of the aircraft. For example, night curfews are loose constraints, because both freight operators and no-frills airlines already use (and lobby to use) night slots. Paying for removal or improvements of properties around the airports will not be financially sustainable.

The purpose of the present study is to address the feasibility of a steep continuous descent approach. The steep descent can also be part of a two-segment final approach, for example, a flight maneuver in which the airplane maintains the conventional level flight for a longer time, before heading down along the ILS glide path at a larger glide slope. In addition to the noise abatement problem, the case of limited access space of the airport is addressed. The procedure can be tested from the point of view of maneuver time and fuel consumption. A steep descent may only need to be performed at particular airports.

A sequence of final approach and landing phases is shown in Fig. 1. In a TMA a commercial jet transport aircraft will start from an altitude around 2800–3000 m (9200–9800 ft) above the airport level, at a speed 400 km/h (215 kn), around 10 nautical miles from the airfield. The final approach is done at speeds around 135–160 kn. The noise certification point is at a distance of 2.0 km (1.08 n miles) from the airfield. A flight path with increased descent rate should not exceed the approach speed of the nominal case. Furthermore, any increase in attitude, aimed at increasing the lift, may compromise the ground visibility at a critical time before landing.

The most important constraint is the flight safety. In the present context it will assumed that safety is not compromised if the terminal

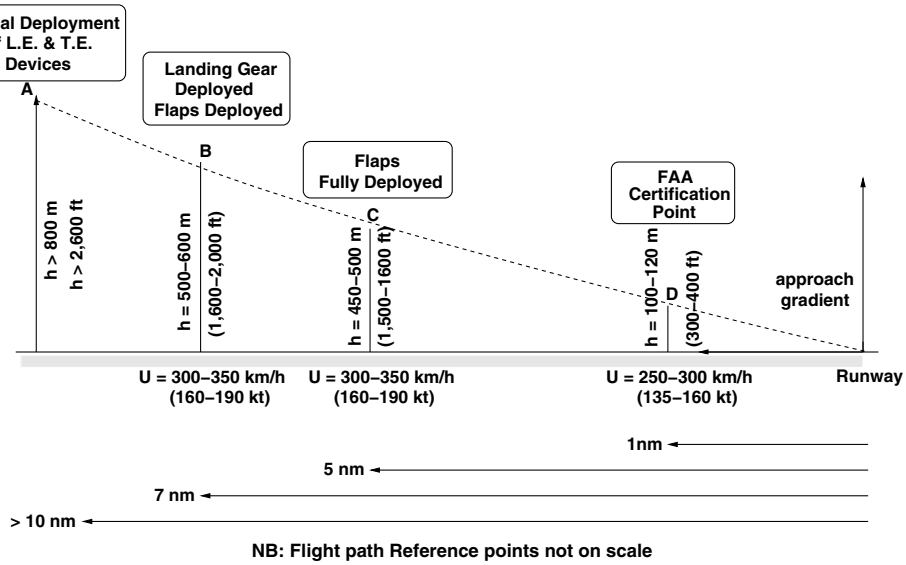

Fig. 1 Sequence of high-lift devices and landing gear deployment.

descent speed is the same as in the nominal flight path. Because this conditions cannot always be enforced, as proved in this study, the maneuver ends conventionally at 100 m (348 ft) above the airport level. Below this altitude the aircraft must gradually reestablish the conventional glide slope. Thus, there shall be no additional consideration for landing gear structural limit. For the sake of generality, a flight in standard atmosphere is assumed. In the present study there is no consideration of externalities, such as winds, side gusts, engine cutoff, and unavailable runway before landing.

The descent speed of the aircraft is

$$v_s = V \sin\gamma \tag{1}$$

By assuming a small angle of gliding, and using the definition of the C_L, v_s becomes

$$v_s = \sqrt{\frac{2}{\rho_o}}\sqrt{\frac{W}{A}}\frac{1}{\sqrt{\sigma}}\frac{1}{\sqrt{C_L}}\frac{C_D^2}{C_L^2 + C_D^2} \simeq \sqrt{\frac{2}{\rho_o}}\sqrt{\frac{W}{A}}\frac{1}{\sqrt{\sigma}}\frac{C_D}{C_L^{3/2}} \tag{2}$$

The slope of the trajectory is

$$\gamma \simeq \sqrt{\frac{2}{\rho_o}}\sqrt{\frac{W}{A}}\frac{1}{\sqrt{\sigma}}\frac{C_D}{C_L^{3/2}}\frac{1}{V} \tag{3}$$

For a fixed weight, a change in the flight path gradient requires a change of the aerodynamic coefficients. If the true air speed (TAS) is unchanged, then an increase in the descent angle would increase the descent speed. This effect could be a hazard. To avoid the problem, a decrease in TAS will be required. If, in fact, v_s is constrained to the value of the nominal flight path, then the TAS must decrease according to

$$V \sin\gamma = \text{const} \tag{4}$$

If the subscript r denotes the reference (nominal) flight conditions, then the ratio between the steep-descent TAS and the reference TAS is

$$\frac{V}{V_r} = \frac{\sin\gamma_r}{\sin\gamma} \simeq \frac{\gamma_r}{\gamma} \tag{5}$$

A doubling of the descent angle implies a halving of the air speed, which can easily lead to catastrophic consequences. Only an aircraft with very high lift and good stall behavior would be capable of performing such a landing. The target set by London City airport corresponds to an increase of the descent angle by about 80%: a formidable goal.

Consider again Eq. (3). Frustratingly, the drag would have to increase faster than $C_L^{3/2}$. Thus, there will be some practical limitations in the descent slope; these are a combination of flight safety, aerodynamic performance with high-lift devices, and overall noise emission. In first instance, the relevant parameter to consider is

$$a = \frac{C_D}{C_L^{3/2}}\frac{1}{V} \tag{6}$$

II. Aircraft Model

The aircraft of reference is the Airbus A310-200. The full aircraft is specified by 60 parameters (dimensions, weights, aerodynamic coefficients); 40 engine parameters (dimensions of various subsystems, basic performance parameters), and up to 20 operational parameters (atmospheric and flight conditions). In addition, tabulated charts of aerodynamics and engine performance are used. The aircraft is divided into major subsystems: main wing, horizontal tail, vertical tail, landing gear (all groups), fuselage, engines. Flaps and slats geometry and settings are required for noise calculations.

The aircraft is powered by two General Electric CF6-80C2. At least 23 versions of this engine exist, each with a different pressure ratio, thrust rating, and emission indices. The engine is simulated with NLR's program GSP, a simulation tool for gas turbine engines developed by Visser and his coauthors at the NLR [6]. A full analysis includes the 1-D steady-state aerothermodynamic properties (pressure, temperature, mass flow) of the gas flow at all sections of the engine. The main parameters examined for the present calculations include thrust, fuel flow, airflow, specific fuel consumption, inlet/outlet combustor temperatures, total pressures at the combustor and power turbine (for engine noise calculations), exit nozzle jet speed and temperature (for jet noise calculations), environmental emissions (NO_x, CO), out of 90 output parameters.

Some engine characteristics at landing are shown in Fig. 2. The data are plotted against the net thrust per engine, because this parameter is calculated in real time by the simulation program. The band shown in the graph indicates the changes in engine performance between sea level and the starting altitude. The lines are polynomial fit of the simulated data; these are used for the jet noise simulation.

The computational model is implemented into a general performance code called FLIGHT. The code includes routines for the calculation of the drag and the drag breakdown, wetted areas, flight performance at all conditions (from taxi-out to taxi-in), and noise models for all major subsystems. The engine simulation from GSP cannot be easily incorporated into the FLIGHT model. Hence, the analysis is done independently, and suitable performance charts are constructed and used as input by FLIGHT. Typically, the output of this code consists of several real-time parameters at all flight conditions. Separate engine charts are used for the steep-descent analysis, due to the different level of detail required for both flight and noise simulation.

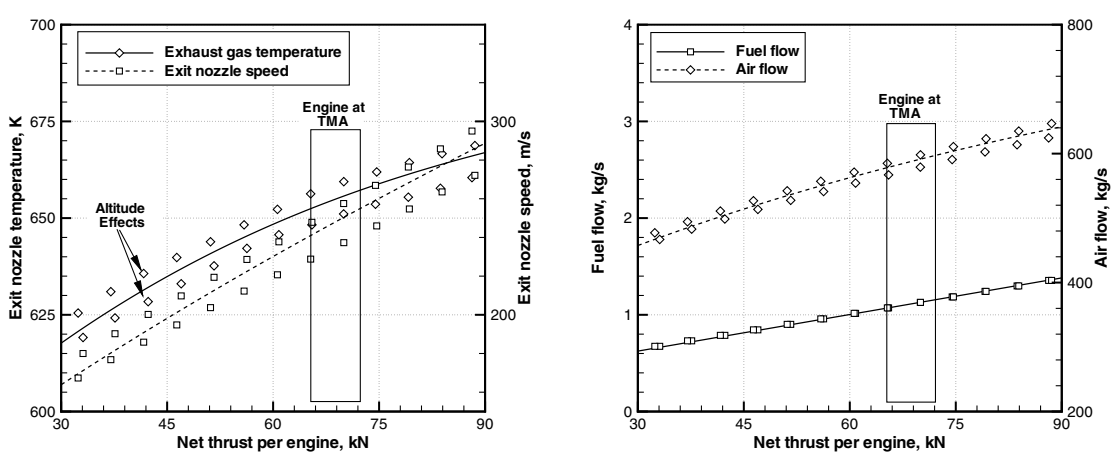

a) b)

Fig. 2 Steady-state simulation of the CF6-80C2 engine at landing.

III. Aerodynamic Performance

At the speeds considered, the parabolic drag equation is a quite accurate description of the aerodynamic drag at cruise conditions,

$$C_D = C_{D_o} + k_1 C_L + k_2 C_L^2 \tag{7}$$

The term C_{D_o} will be discussed further in Sec. V. Increasing or decreasing the effective lift coefficient requires to increase or decrease the attitude, but it can also be achieved by extending the leading- and trailing-edge control surfaces. At incidence, the fuselage contributes to the lift, as well as drag. Any increase in lift is associated to an increase in drag. This behavior is quite general, and is discussed by Flaig and Hilbig [7] for the Airbus family of commercial airplanes.

Let us define the *descent factor*

$$f_d = \frac{C_D}{C_L^{3/2}} = \frac{C_D}{C_L}\frac{1}{C_L^{1/2}} = \frac{1}{C_L/C_D}\frac{1}{C_L^{1/2}} \tag{8}$$

and study the aerodynamic performance in terms of L/D and f_d. Before proceeding, note that f_d also appears in classical minimum-power problems. Minimum level flight power is ensured by minimum f_d. In the present case one is concerned with the *maximum* f_d.

An example of descent factor is shown in Figs. 3 and 4 for the Airbus A-310 ALVAST model in scale 1:10. The wing of the A-310 is similar to the wing of the A-300-600 (a larger aircraft). In particular, these aircraft have nearly the same leading-edge slat: the A-300 has a single-slotted flap; the A-310 has a single-slotted flap inboard and a double-slotted flap outboard.

The data of Figs. 3 and 4 have been extracted from Kiock [8]. Computational fluid dynamics (CFD) calculations for this configuration have been shown by Rudnik et al. [9]. Therefore, the data have been extensively validated. These data will be assumed representative of the full-scale aircraft.

The descent factor f_d reaches a minimum at intermediate values of C_L. To guarantee a relatively high descent rate, the aircraft will have to operate at $C_L \simeq 1$. With this value of C_L, the glide ratio is suboptimal, albeit close to the maximum for this particular configuration, $L/D \simeq 8.7$. Beyond this value, there is a decrease of the descent factor f_d, which is the defining parameter, along with the air speed [Eq. (6)]. Looking at the problem from another point of view, a large descent rate would require to operate the aircraft at a C_L about double its cruise value, but far from the maximum C_L. At a given TAS, operating the aircraft around $C_{L_{\max}}$ produces a low descent rate: an obvious result.

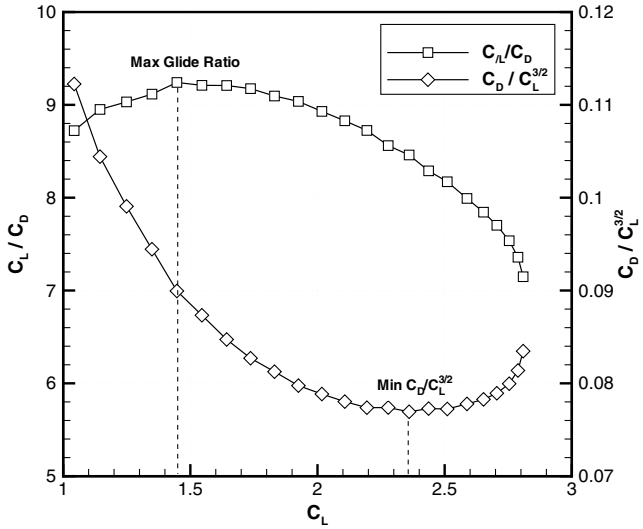

Fig. 4 Glide ratio and descent factor f_d [Eq. (8)] of the Alvast/A-310 scale model wing.

At landing configuration, the best quadratic fit of the wind tunnel data is

$$C_D = 0.127556 - 0.056755 C_L + 0.051947 C_L^2 \tag{9}$$

The data shown refer to a *single configuration* of the wing. These data are by themselves not enough to elaborate on the performance of a wing system with a step change in the deployment of the high-lift devices. However, some cautious extrapolations can be done. From the analysis of experimental data on straight wings equipped with trailing-edge flaps (for example, Johnson and Hagerman [10]), it was found that the shape of the parameter f_d is similar to that shown in Fig. 4. For a given value of the C_L, f_d increases with the increasing flap deflection δ_f. This effect is shown in Fig. 5, for a straight wing of aspect ratio 3.13 equipped with a full-span flap. The line shown in the graph is a quadratic fit that has the form of Eq. (7).

When the coefficients of this equation are plotted at different flap settings, it is found that C_{D_o} is nearly constant; k_1 increases with the flap angle δ_f, and k_2 decreases with δ_f, as shown in Table 1. Therefore, the change in drag is essentially due to the pressure drag created by the flow deflection, and ultimately by the flap setting.

If the same reasoning is applied to the aerodynamic data at landing [Eq. (9)], it is estimated that the nonlifting portion of drag coefficient

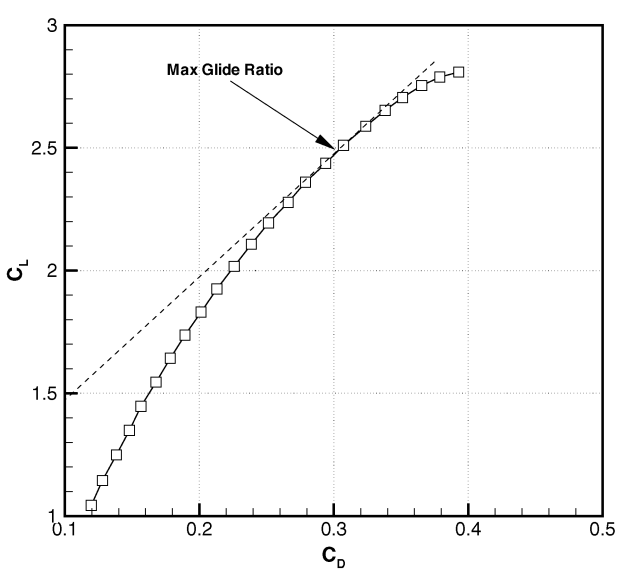

Fig. 3 Drag polar of the Alvast/A-310 scale model wing, takeoff configuration.

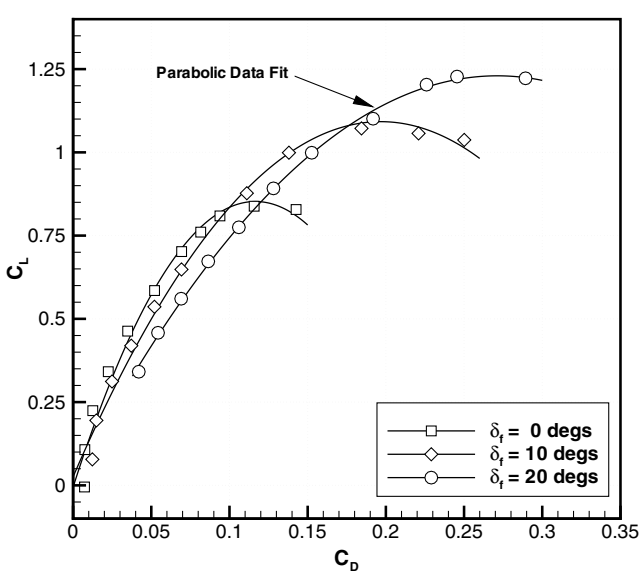

Fig. 5 Drag polar of a straight wing at three positions of the flaps. Elaborated from Johnson and Hagerman [10].

Table 1 Parabolic interpolation of Eq. (7) for the straight wing of aspect ratio 3.13

δ_f	C_{D_o}	k_1	k_2
0	5.403963×10^{-3}	1.471623×10^{1}	-6.311658×10^{1}
10	2.577274×10^{-2}	1.084435×10^{1}	-2.756782×10^{1}
20	1.025446×10^{-2}	8.991863×10^{0}	-1.657339×10^{1}

is about $C_{D_o} \simeq 0.128$, and depends only weakly on the C_L. From this result, one can investigate the changes in landing performance created only by changes in the C_{D_o} of the aircraft.

For moderate values of the C_L the L/D decreases almost linearly with the increasing C_L. This means that polars like those in Fig. 3 can be rescaled. Unfortunately, the polars discussed do not have any implication on the steep descent. First, at $C_L \simeq 1$ the descent rate could be too high, therefore the aircraft would have to limit the f_d by increasing its C_L. Second, if this is not the case, the use of a moderate C_L creates the conditions for maximum descent rate at a given air speed. The results is that, as the descent rate is increased, flight safety is compromised. To avoid this risk, the air speed has to decrease; to maintain the aircraft at a speed above the stall speed, the C_L has to increase. These are conflicting requirements.

Now the problem is formulated as follows. Fix the flight path with a specified slope. The aircraft is to move along this trajectory from the initial altitude, so that at the final altitude the descent rate is below a threshold value considered safe:

$$v_s < v_{s_r} \tag{10}$$

On the other hand, from Eq. (2) the ratio between descent rate in the steep and nominal flight path is

$$\frac{v_s}{v_{s_r}} = \frac{f_d}{f_{d_r}} \tag{11}$$

A similar condition for the airspeed [derived from Eq. (2)] is

$$\frac{\gamma}{\gamma_r} = \left(\frac{V_r}{V}\right)\left(\frac{f_d}{f_{d_r}}\right) \tag{12}$$

or its inverse, when the approach slope is assigned,

$$\frac{V}{V_r} = \left(\frac{\gamma_r}{\gamma}\right)\left(\frac{f_d}{f_{d_r}}\right) \tag{13}$$

One condition is redundant. Equation (13) is used, because it leads to a more direct consideration of the stall speed. Equation (13) must be solved with the constraint

$$V \geq k_s V_{\text{stall}} \tag{14}$$

which in nondimensional form becomes

$$\frac{V}{V_r} \geq k_s \frac{V_{\text{stall}}}{V_r} \tag{15}$$

This limit is slightly more restrictive than the one required by the Federal Aviation Regulations (Sec. 25.103). Finally, the stall speed is defined as

$$V_{\text{stall}} = \sqrt{\frac{2}{\rho}\frac{W}{A}}\frac{1}{\sqrt{0.95 C_{L_{\max}}}} \tag{16}$$

The maximum C_L can be changed by operating on the high-lift surfaces, but it does not change if one only operates on the profile drag. To this end, one needs to solve Eq. (5) with the constraint Eq. (15) and the definition Eq. (16). With a fixed configuration, there is little change in the V_{stall} due to air density. A parametric analysis is shown in Fig. 6.

The horizontal line denotes the stall constraint, Eq. (16). A ratio V/V_r below this line is not an acceptable solution. The other

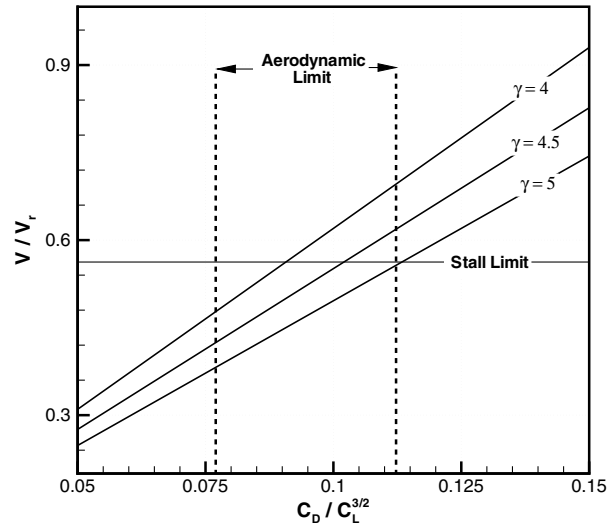

Fig. 6 Parametric behavior of Eq. (11).

constraint is the band delimited by the two vertical lines, $0.078 < f_d < 0.115$, which is the aerodynamic limit of the aircraft in the landing configuration shown in Fig. 4. The wing system cannot provide a value of f_d below or above this band. Therefore, the flight is strongly constrained. It is evident that a descent with a slope $\gamma = 5.0$ deg is not possible. A descent at $\gamma = 4.5$ deg is only possible if the aircraft operates at low C_L, as implied by Fig. 4. However, there is a narrow band in the aerodynamic performance that allows a descent at $\gamma = 4.0$ deg. To extend the descent envelope, the aircraft will have to provide values of

$$f_d = C_D/C_L^{3/2} > 0.12$$

In other words, the aerodynamic limit indicated in Fig. 6 will have to shift to the right of the scale. The next problem is to examine in detail how this can be achieved. There are four possibilities: 1) increase the C_{D_o} at given C_L, 2) decrease the C_L at fixed C_{D_o}, 3) increase the C_{D_o} and decrease the C_L at the same time, and 4) increase both C_{D_o} and C_L, with the condition that f_d increases. The latter case is discussed separately.

A. Increased Zero-Lift Drag

Consider first the case in which one is able to increase the C_{D_o}, by means of clam shells, air brakes, vortex generators, or other devices, applied on the wing, on the fuselage, or both. The flight path is assigned. With the reference data of Eq. (9) calculate the ratio

$$\frac{C_D}{C_{D_r}} = f(C_L) \tag{17}$$

For a doubling of C_{D_o}, Eq. (17) varies from about 2 at $C_L \simeq 1$ to about 1.35 near stall. If the C_{D_o} is increased by 50% over the reference value, the total drag of the aircraft increases by 55% at $C_L \simeq 1$, and by only 40% near stall. In conclusion, as the C_L increases, the effect of increasing the C_{D_o} is reduced.

The second aspect is represented by the behavior of the descent factor. This is plotted in Fig. 7 for parametric values of the C_{D_o}. This result shows again that it is not convenient to operate at large C_L to increase the descent rate, due to the power 3/2. On the contrary, an intermediate value of $C_L \simeq 1$–1.2 provides sufficiently high value of the descent factor. Therefore, the aircraft will have to operate at this level of the lift, while attempting to increase its profile drag as much as required to perform a steep descent.

With the additional drag, a higher thrust is required to maintain the air speed. However, if the aircraft starts from an air speed suitably higher than V_{stall}, there is a margin in which the aircraft can be allowed to decelerate, by using less thrust. As a result, also the descent rate can be reduced, to comply with Eq. (2).

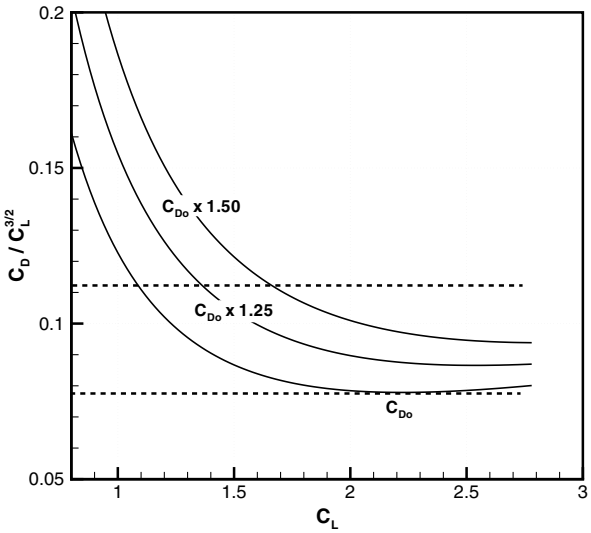

Fig. 7 Effects of C_{D_o} on the descent factor f_d, Eq. (8), at landing configuration.

B. Variation of Both C_{D_o} and C_L

The profile drag increase required for a prescribed steep descent can be excessive. The difficulty can be overcome by decreasing the lift, as well as increasing the drag.

Let us do a closer examination of the descent factor. Study the change in f_d due to a combined change in C_{D_o} and C_L, by writing the ratio

$$\frac{f_d}{f_{d_r}} = \frac{C_{D_o} + k_1 C_L + k_2 C_L^2}{(C_{D_o} + k_1 C_L + k_2 C_L^2)_r} \left(\frac{C_{L_r}}{C_L}\right)^{3/2} \tag{18}$$

Now call $x = C_L / C_{L_r}$ the relative lift coefficient. By dividing Eq. (18) by $C_{L_r}^2$, one finds

$$\frac{f_d}{f_{d_r}} = \frac{c_1 p + k_1 x / C_{L_r} + k_2 x^2}{c_1 + k_1 / C_{L_r} + k_2} x^{-3/2} \tag{19}$$

with $c_1 = (C_D / C_L^2)_r$ a fixed parameter, and $p > 1$ a factor of the profile drag over the nominal condition. Equation (19) does not contain any constraint on thrust or air speed.

In Fig. 8 the relative lift descent factor (right axis) is plotted vs the relative lift, and the relative profile drag (left axis) vs the relative lift. The reference point is indicated by R. Assume that the C_L decreases by 36%, while keeping the same profile drag. The operation point in the chart of Fig. 8 is A. This point corresponds to an increase in descent factor by about 50%. The total drag decreases by 20% (right-hand scale from point A′). At constant TAS, the descent angle would increase from 3 to 4.5 deg. If, instead, the zero-lift drag is increased by 25%, to achieve the same gain in descent factor (point B), the lift would have to decrease by 24.5%, a more modest value, though still quite high. In this case the drag would increase by a modest 6%. If the air speed has no stall constraint (although this can be verified at a later stage), it is possible in principle to achieve a 50% increase in descent angle by a combined 50% increase in drag and 20% decrease in lift (point C in the graph).

If the drag Eq. (9) is modified by increasing the zero-lift drag by the required 50%, then the practical aerodynamic limits of the wing system provide a descent factor

$$0.18 < f_d < 0.25$$

This band is moved to the left of the graph in Fig. 6.

IV. Aerodynamic Design

The aerodynamic performance of the aircraft will have to be modified to take into account new constraints arising from a steep-descent flight path. Starting from a second-order curve fit of the Alvast model

$$C_L = C_{D_o} + k_1 C_L + k_2 C_L^2 \tag{20}$$

upgrades to the aerodynamics are done by using an equation such as

$$C_L = p C_{D_o} + p_1 k_1 C_L + p_2 k_2 C_L^2 \tag{21}$$

where $p \geq 1$, and p_1, p_2 are free parameters. The equation is still a second-order polynomial (using higher-order polynomials might not be a good idea, because the role of the profile drag is not evident). The free parameters must be chosen so that

$$C_{L_{\max}} > C_{L_{\max}}^* \tag{22}$$

$$f_d > f_d^* \tag{23}$$

$$C_{D_o} \geq C_{D_o}^* \tag{24}$$

This is a problem of nonlinear programming. The unknowns are p, p_1, p_2. The solution can be simplified if one sets $p_1 = p_1 c$ and $p_2 = p_2 / c$, with c a constant factor. This problem cannot be discussed in detail in this context for the sake of brevity. However, the domain of possible solutions is shown in Fig. 9. The solution is

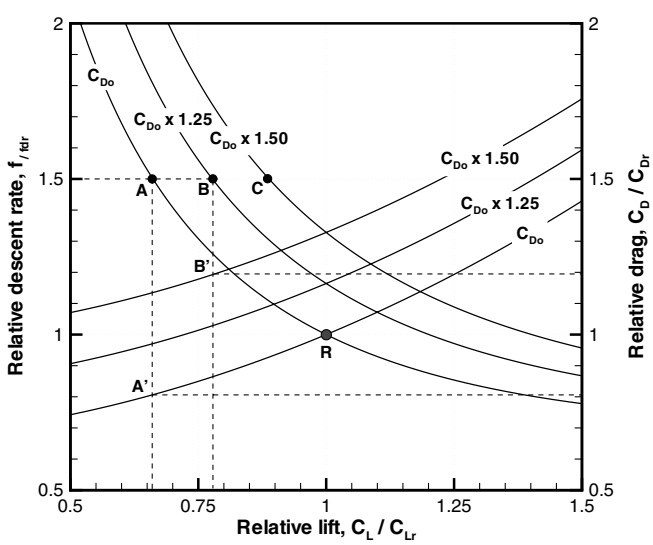

Fig. 8 Combined effects of zero-lift drag and lift coefficient on the relative descent rate.

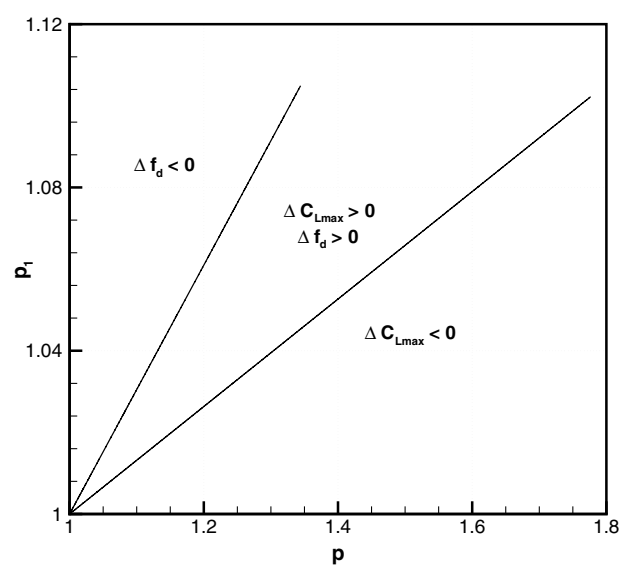

Fig. 9 Solution of Eq. (21).

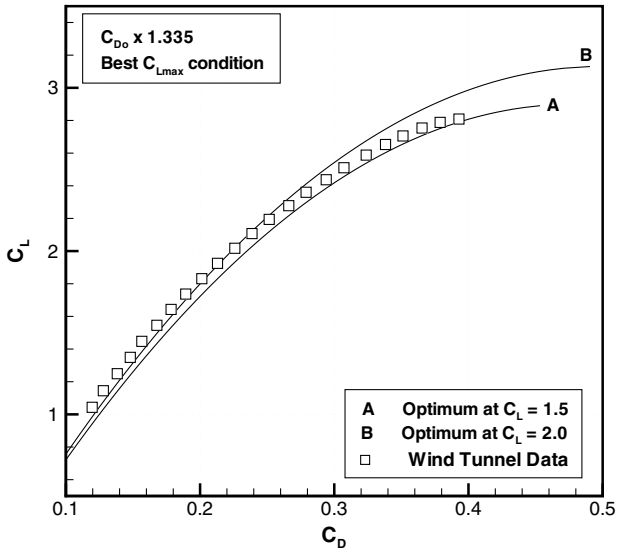

Fig. 10 Modified drag polar.

the central wedge from the nominal point at the vertex. At the nominal profile drag, any change in k_1 and k_2 cannot improve $C_{L_{\max}}$ *and* $C_D/C_L^{3/2}$ at the same time. Therefore, an increase in profile drag ($p > 1$) is required. In the solution domain there is no absolute optimum. A number of interim conclusions are in place: 1) the best $C_{L_{\max}}$ is found at a point (p, p_1, p_2) different from the point of best f_d, 2) the increase in $C_{L_{\max}}$ is lower than the increase in f_d, 3) the increase in $C_{L_{\max}}$ and f_d is limited by the upper bound on C_{D_o}, 4) the gain is reduced at high-lift coefficients, and 5) moving along the lower limiting line improves f_d, rather than the $C_{L_{\max}}$; conversely, moving along the upper limiting line it improves $C_{L_{\max}}$, rather than the f_d.

An increase in aerodynamic performance will be limited by the practical limitations on the profile drag. The possibilities increase with the increasing profile drag. Furthermore, the improvement depends on the C_L. Operating at values above or below a certain C_L may deteriorate the aerodynamic performance, rather than improve it. Constraining the problem at all C_L complicates the matter. This problem was left behind for further investigation.

Figure 10 shows a solution with $\Delta C_{L_{\max}} \simeq +7\%$ at $C_L = 1.5$, and $\Delta C_{L_{\max}} \simeq +5.2\%$ at $C_L = 1.5$; the C_{D_o} is increased by 33% in both cases. Figure 11 shows a solution with $\Delta f_d \simeq +14.5\%$ at $C_L = 1.5$, and $\Delta f_d \simeq +8.2\%$ the C_{D_o} is increased by 33%.

The cases presented indicate that there is an improvement in aerodynamics at selected C_L. Operating at large C_L may be

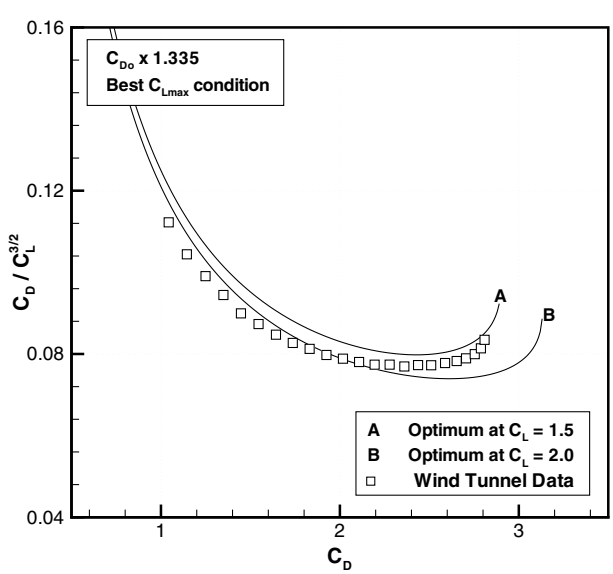

Fig. 11 Modified descent factor.

detrimental, as previously discussed. A further increase in C_L is difficult to obtain in practice, although the parametric analysis shown here can produce larger $C_{L_{\max}}$. The optimal descent solutions (as described in the next section) require an increase in C_L as the aircraft loses altitude. Therefore, stall situations occur near landing.

The foregoing analysis was limited to a $C_{L_{\max}}$ below 3, which is the largest value achievable with the current technology of unpowered high-lift devices. The use of vectored thrust or externally blown flaps would allow more control. However, this technology is not available in the present generation of transport aircraft.

V. Drag Breakdown

The next step is to identify the sources of drag, and to figure out where an increase in profile drag can be achieved, and how much it is realistic to expect.

For a modern subsonic jet transport, the profile drag corresponds to an average 40–50% of the total drag in cruise conditions. The contribution of the fuselage and the wing to this drag component is estimated from Torenbeek [11]. The drag breakdown is

$$C_{D_o}A = c_{Re}c_{\mathrm{lg}}[(C_DA)_w + (C_DA)_f + (C_DA)_{\mathrm{tp}} + (C_DA)_e] \tag{25}$$

that includes the contributions of the main wing, the fuselage, the tailplane, and the engines, respectively. The area A on the left-hand side is the reference wing area; the factor c_{Re} is a correction for scale effects, surface roughness, interference, trim and other causes. Torenbeek provides a correlation between this factor and the Reynolds number based on cruise conditions

$$c_{Re} = \frac{47}{Re^{-0.2}} \tag{26}$$

The factor c_{lg} is a correction for landing gears deployed. With landing gears inside the hold, $c_{\mathrm{lg}} = 1$. Equation (25) does not include the effects of base flow separation, particularly at the final stage of the approach, when the aircraft flares up. The wing drag is

$$(C_DA)_w = 0.0054r_w[1 + 3(t/c)\cos^2\Lambda_{\mathrm{qc}}]A \tag{27}$$

where t/c is the average wing thickness and r_w is a factor that for the aircraft of reference can be considered equal to one. The tailplane drag is calculated as the wing drag.

The average skin friction coefficient is calculated from Schultz and Grünow (as reported by White [12]), on the basis of a reference Reynolds number. The contribution of each fuselage section is calculated according to the wetted area. The base pressure drag is calculated according to a semi-empirical formula provided by Hoerner [13]. The combination of these factors gives a skin friction drag of about 70% and a pressure (base) drag of about 30% at landing conditions. This drag breakdown should also indicate where a drag rise is possible. The analysis is shown in Fig. 12.

The engine drag is

$$(C_DA)_n \simeq 2.58\frac{5 + \mathrm{BPR}}{1 + \mathrm{BPR}}\frac{T_{to}}{\psi p_o} \tag{28}$$

where BPR is the bypass ratio, p_o is the standard atmospheric pressure, and ψ is the ratio between the net thrust and the airflow.

With this analysis one finds that the profile drag of the wing is comparable with the profile drag of the fuselage, $(C_{D_o})_f \simeq 1.06(C_{D_o})_w$. The profile drag of the tailplane is about 12% of the main wing, $(C_{D_o})_{\mathrm{tp}} \simeq 0.12(C_{D_o})_w$; the total engine drag is $(C_{D_o})_e \simeq 0.04(C_{D_o})_w$. Therefore, for this particular case the wing's profile drag is equal to 45% of the total profile drag.

A detailed breakdown of the profile drag for the Airbus A-310 is given by Haftmann et al. [14] and can be summarized as follows: 32.3% is due to the fuselage, 22.8% is due to the wing, 13.7% is due to the tail surfaces (fin, rudder, elevator), and 4.3% is due to the engines. The configuration analyzed by Haftmann et al. includes flaps and slats, which adds another 18.8% to the drag count. If this

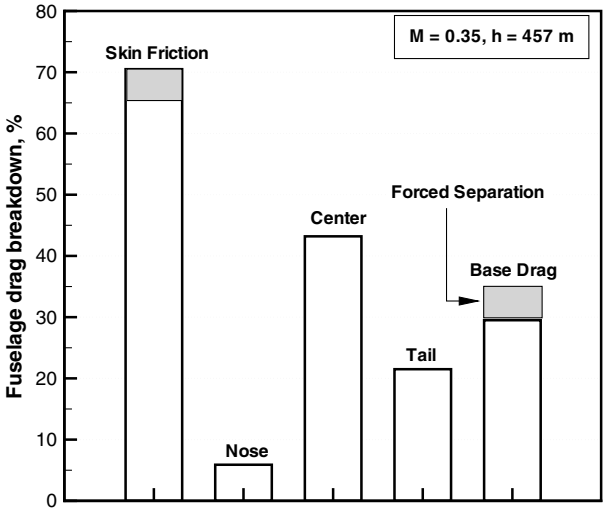

Fig. 12 Fuselage drag breakdown.

figure is added to the main wing, one would have about 41.6%, a datum close to our first-order estimation.

Increasing the C_{D_o} by 25% by operating on the wing alone would require increasing the wing drag by 55%. Increasing the C_{D_o} by 50% would require to more than double the wing's drag (the correct value should be around 210–215% of the reference value).

Solutions that operate on the high-lift devices and the wing require to increase the drag and decrease the lift. This could be done with appropriate vortex generators, whose function is to disturb the attached flow on the wing and to create a partial and controlled flow separation. A number of technologies have been already explored for the manipulation of the profile drag, including microdrag generators on the wing (Bauer [15]). The shaded area in Fig. 12 shows an estimate of the contribution of the base drag if flow control were applied in the aft fuselage.

Solutions that operate on the airframe alone must be some kind of air brakes. The decrease in lift could be obtained by a change in attitude of the aircraft. Therefore, the combination of the two factors could force the aircraft to drift down at a faster rate. Solutions of this nature include the clam shells previously discussed. The use of aerodynamic decelerators, such as parachutes, is not deemed appropriate for this type of aircraft.

VI. Steep-Descent Solutions

Consider now the effects of the aerodynamic coefficients for the aircraft, to find the most suitable aircraft configuration for increasing the approach gradient. There are two ways to solve the problem: one is to fix the trajectory, and another is to calculate the trajectory corresponding to the flight inputs. In the latter case, the flight path is governed by the following differential equations:

$$m\frac{dV}{dt} = T - D - W\sin\gamma \tag{29}$$

$$m\frac{v_s}{dt} = (T - D)\sin\gamma + W\cos\gamma \tag{30}$$

$$\tan\gamma = \frac{v_s}{V} \tag{31}$$

$$\dot{m}_f = f_j D \tag{32}$$

In the present analysis the flight path angle is assigned. The flight is formulated as a two-value boundary problem by three differential equations (flight path and all-up-weight), four algebraic constraints (stall speed, required thrust, engine throttle, descent rate at the terminal point), one integral constraint (noise emission), and three free parameters (C_{D_o}, C_L, and initial TAS). The algebraic constraints are

$$V > k_s V_{\text{stall}} \tag{33}$$

$$T < T_{\text{av}} \tag{34}$$

$$[v_s]_2 \leq [v_{s_r}]_2 \tag{35}$$

$$\Pi = \Pi_{\min} \tag{36}$$

In these equations T_{av} is the net thrust available at a given air speed and flight altitude, 2 is the terminal point for the maneuver (100 m; 348 ft), $\Pi_{\min}$ is the minimum throttle setting compatible with the assigned flight trajectory. This limit is part of the solution. It is calculated at the start of the maneuver, and then kept constant. If $\Pi_{\min}$ were to be calculated at every step, then another degree of freedom would be introduced. Note that a terminal constraint on the rate of descent is also a terminal constraint on the air speed. The solution strategy attempts to comply with all the constraints.

The previous analysis is used to elaborate on the most appropriate changes in C_{D_o} and C_L. This means that initially the flight was simulated with the nominal drag polar and then with appropriate changes in the aerodynamic coefficients. The noise emission simulation method is discussed separately. However, in the present procedure the noise simulation is not used directly as a constraint; rather, it is used to verify the noise level at reference points.

Under nominal conditions, a decrease in air speed of the order of 30 kn is achieved in this maneuver. A number of options can be considered. The flight path can be thought of as made up of two segments. First, the thrust is reduced as the drag is increased. The aircraft drifts down and loses TAS. When the TAS has reached a control value [Eq. (15)], the aircraft moves along the prescribed trajectory. For a descent at $\gamma = 5.5$ deg, the TAS required to maintain the same value of the descent rate would have to decrease by 83%: an unlikely prospect. The second option is to decelerate uniformly from the initial TAS (generally around 220 kn) to a final TAS, to comply with a terminal descent rate equal to that of the nominal flight path [Eq. (35)]. Therefore, the problem's equations and constraints are solved iteratively around the manoeuvring time. The procedure converges in three to four iterations. The initial conditions ($t = 0$) are γ_o, V_o, γ_o, W_o, with the aircraft at the reference position $h = h_o$, $x = 0$.

Figure 13 shows the descent performance at nominal conditions. In the attempt to reduce the speed to meet the terminal constraint on

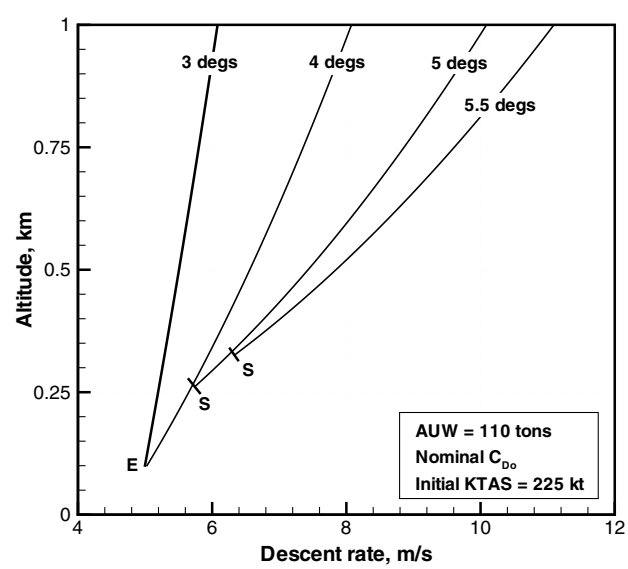

Fig. 13 Steep descent with nominal aerodynamic performance.

the descent rate, the aircraft is forced to stall as the slope of the trajectory is increased (point S in the graph). The example shown refers to a relatively high weight for this aircraft. The effects are mitigated by decreasing landing weight, albeit not to a level that would overcame the stall.

At least six different remedies have been investigated:

1) Relax the terminal constraint, and allow the terminal descent speed to be higher.

2) At the incipient stall maintain a constant TAS and allow the aircraft to descend along a more shallow trajectory.

3) At the incipient stall, accelerate in level flight, then perform a final descent.

4) Improve the aerodynamics (e.g., the drag polar).

5) Use vectored thrust to augment the lift.

6) Start the steep descent from a lower altitude (typically, 1500 ft).

Some of these results are shown next.

Figure 14 shows the descent performance of the aircraft with a relaxed terminal constraint. Mathematically, this meant that the terminal v_s was the minimum compatible with a descent along the specified flight path. The constraint had to be relaxed particularly on the $\gamma = 5.5$ deg. For this case, the final $v_s \simeq 6.7$, instead of 5.0 m/s. This allows for an increase of v_s by 34%.

Figure 15 shows the descent performance for the case in which the aircraft reverts to constant true air speed in knots (KTAS) at the incipient stall. Below this altitude, the aircraft maintains the specified slope, but the terminal constraint on the descent speed is violated. However, this case is not as severe as the previous one. The final v_s was about 6 m/s, only 20% higher than the nominal case.

Figure 16 shows the descent performance for the aircraft starting from a lower altitude. The initial point of the trajectory was set at 1500 ft (457 m). A comparison is made between a descent with a relax of the terminal constrain, and a descent at constant TAS at incipient stall.

The weight is not a clear determinant of the descent performance, although the aircraft would tend to stall later as it becomes lighter. However, within the range of weights considered for the model aircraft, a lower landing weight does not solve the problem. The result can be inferred from Fig. 17. Anyway, it is likely that certification to operate a steep descent will have to be done at the maximum landing weight.

The steep-descent solution at the target $\gamma = 5.5$ deg shows a number of other important aspects; first of all, the ratio between the nonlifting drag and the total drag. This parameter is plotted in Fig. 18. This result is relative to an increase of 25% of C_{D_o} over the baseline, and indicates that the nonlifting drag is relatively low; also, it decreases as the aircraft increases its lift and approaches stall. The drag itself (not plotted) is in the range of 122–123 kN.

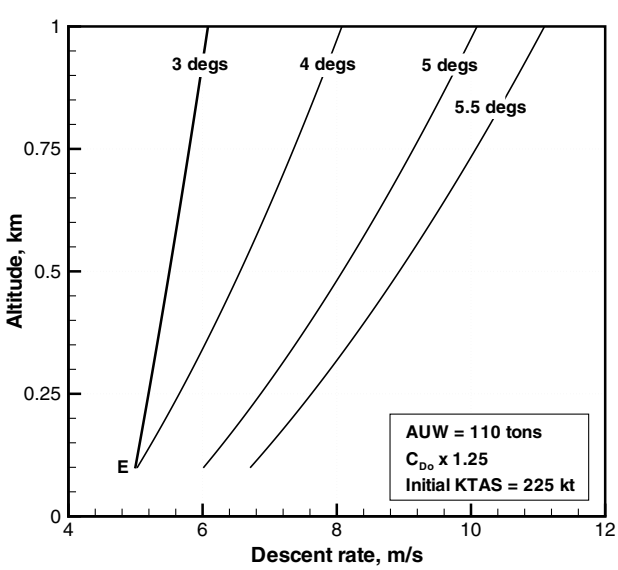

Fig. 14 Steep descent with relaxed terminal constraint.

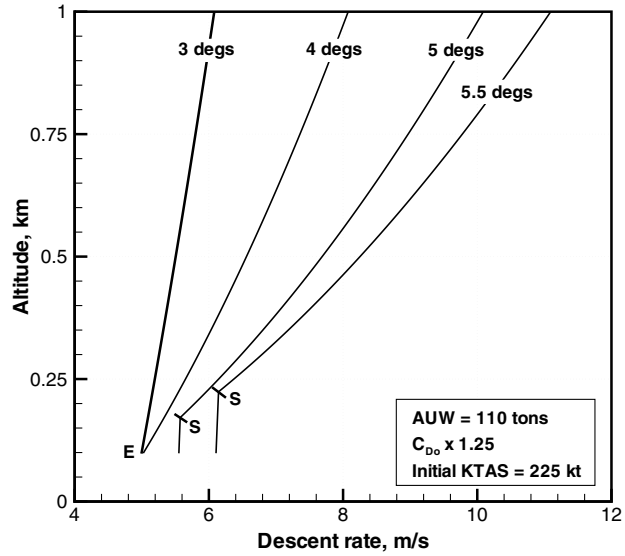

Fig. 15 Steep descent with constant KTAS before stall.

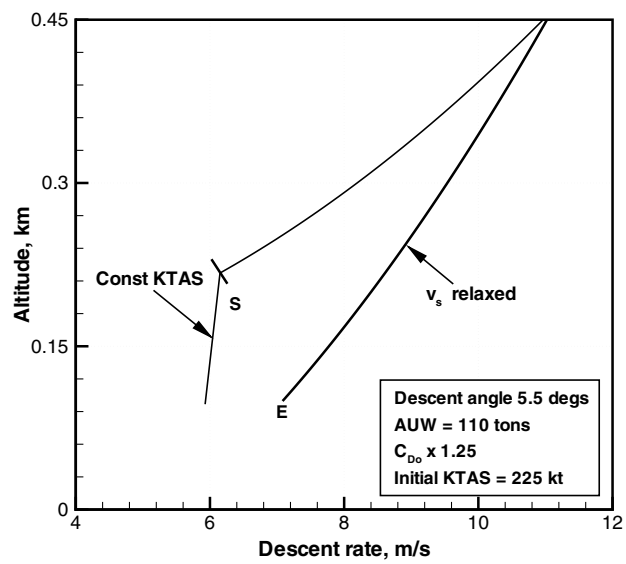

Fig. 16 Steep descent with start at 457 m (1500 ft).

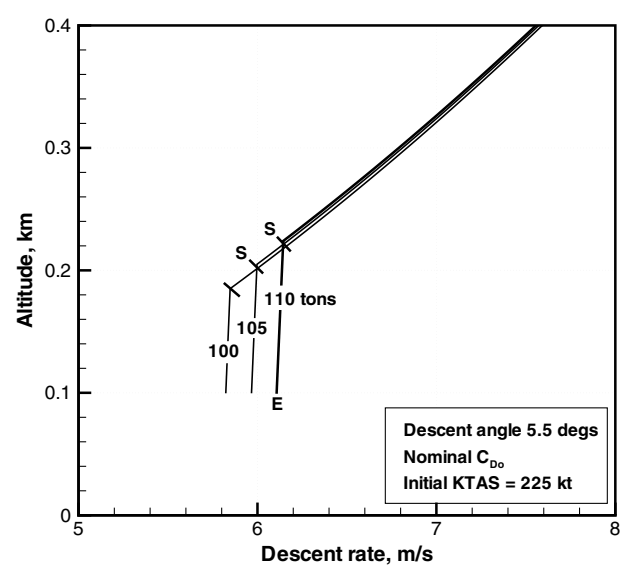

Fig. 17 Effects of all-up weight (AUW) on the descent performance, $\gamma = 5.5$ deg.

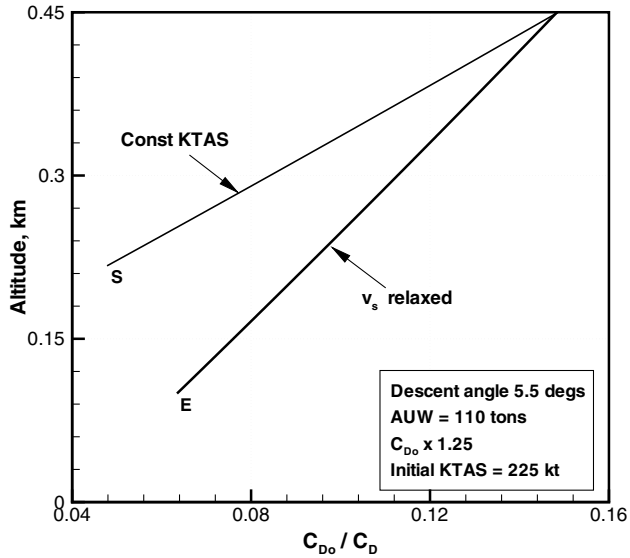

Fig. 18 Nonlifting drag as a proportion of the total drag

Therefore, assuming an average nonlifting drag of the order of 14% at lower altitudes, it leads to $D_o \simeq 16$ kN. Hence, the 25% increase in C_{D_o} is an increase in drag by 3.2 kN: a result that can be achieved.

The second aspect is concerned with the thrust required to operate the aircraft along the specified flight path and with the terminal constraints discussed earlier. With reference to the results of Fig. 18, and the analysis of the minimum thrust required in the nominal flight path, a general increase in throttle is required. This result is due to an increased drag, coupled with a larger air speed. In other words, to maintain a given speed with an increased drag the thrust must increase.

The time history of the maneuver is shown in Fig. 19. The parameters plotted are the C_L, the descent factor f_d and the angle of attack of the aircraft α, and the pitch attitude. In particular, the descent factor is decreased with the increasing descent slope. This is due to the fact that the aircraft operates at C_L levels below the ones that have been used to optimize the aerodynamic performance (refer to Fig. 11). It was also indicated that an improvement on f_d over the entire C_L range is difficult, and was left out for further investigation.

A number of other conclusions are available. First, the steep descent at $\gamma = 5.5$ deg saves about 60 s for a start at $h = 1000$ m (3048 ft), compared with a maneuver at the nominal descent path. The maneuver time is understood as the time from the initial altitude and air speed to the final altitude (and whatever final speed is possible to achieve). This calculation does not provide credit for the time required to fly the extra distance at the top of descent. This extra distance is credited to the flight time, rather than the descent maneuver. Furthermore, the maneuver time depends on the descent strategy that avoids aircraft stall. The case considered refers to a flight

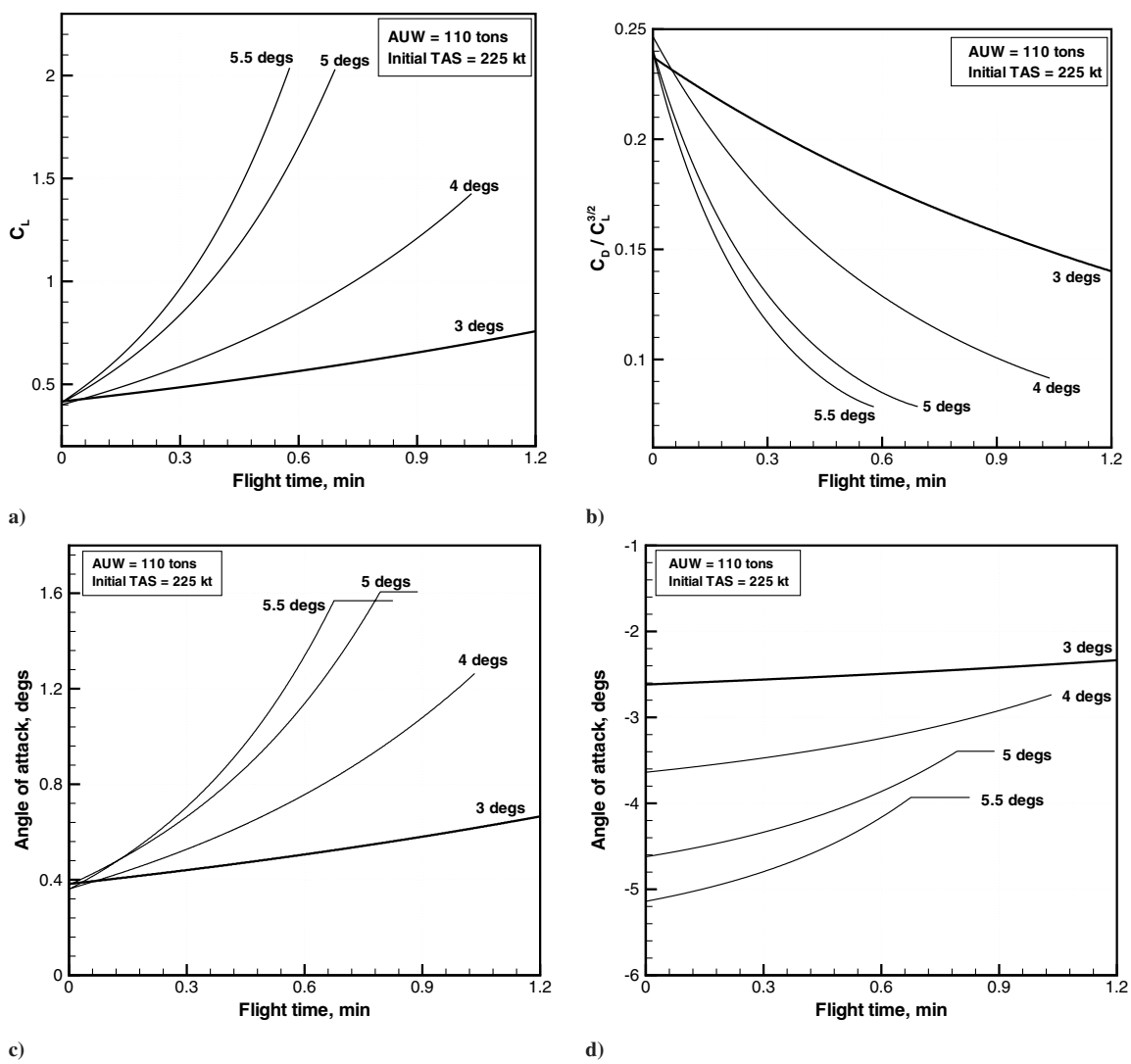

Fig. 19 Time histories at different descent slopes.

at constant TAS before stall occurs, as shown in Fig. 15. The result would be different for a strategy that allows a relax on the terminal descent speed.

If a noise reduction can be associated to this maneuver (as proved in the noise analysis), the result translates into an *increased* traffic capability at the airport. This is of considerable consequence at those airports whose environmental compatibility, and future expansion are legal constraints (see for example, Amsterdam Schipol).

VII. Noise Effects

The noise effects due to the increased profile drag can be attributed to two causes: increased airframe noise (due to increased drag) and increased engine noise, due to the increased thrust that is required to maintain the same TAS as the nominal case.

However, when the aircraft is approaching on a steeper gradient it will be further from the reference point at which approach noise certification is done. Therefore, there will be conflict between decreased noise due to steeper approach gradient and increased noise due to increased thrust and airframe noise. The undercarriage noise remains substantially the same. It is assumed that the undercarriage is deployed at the same altitude as in the nominal case.

The aircraft is simulated as a grouping of noise sources calculated through the use of empirical relations. The noise sources are engines (including fan, compressor, combustor, core, and jet-mixing noise), airframe (including flaps), and undercarriage. The method used is based on the "components" concept, like NASA's code ANOPP (see, for example, Fink [16] and Fink and Schlinke [17]).

A flow chart showing the noise simulation model is reported in Fig. 20. The data required to run the noise simulation include weight, atmospheric conditions at aircraft's position, engine data (such as exit nozzle area, rotor-stator spacing, fan dimensions, rpm, number of fan blades, fan design point, jet velocity, mass flow through the fan, mass flow through the core, cycle temperatures, and pressures), airframe data (such as wing area, horizontal tail area, vertical tail area, flap area, wing span, horizontal tail span, vertical tail span, and flap span), and gear data (such as strut/wheel sizing, gear configuration, number of undercarriage units, and track angle).

ESDU [18] provides semi-empirical correlations for most airframe components. This document uses the geometry factors, the length scales, spectral functions, directivity functions, Strouhal numbers, and Doppler effects. Flap deflection and span are considered side by side with the number of sections used to extend the flaps. The airframe noise frequency band is limited to 4 kHz.

The landing gear is also considered in [18]. However, a more detailed calculation was found in the work of Guo [19]. Therefore, this source of noise was excluded from under the airframe "banner." Guo presented a semi-analytical and semi-empirical method. Dimensions of every part of the landing gear external to the aircraft skin are used. Conveniently, Guo's model focuses on an undercarriage similar to the present model aircraft.

The engines are simulated using semi-empirical relationships again derived from ESDU [20–22]. The sound pressure is converted into far-field noise through the calculation of frequency variance, directivity of the noise, and the Strouhal number. The engine noise band is limited by 10 kHz.

The core (or combustor) noise depends on temperature and pressure rise across the core, as well as the flight speed and the mass flow. Additionally, the turbine exit temperature is used, due to the fact that core noise also takes into account the noise generated as the air dissipates through the turbine. The model used [22] allows for the engine setting, the angle between engine exhaust axis, direction of sound propagation, and the angle between aircraft flight path and the engine's axis.

The model for coaxial jet noise relies on a database whose accuracy has been verified within the 30–120 deg angle between engine's axis and receiver. At azimuth angles beyond this range, an extrapolation was done. Jet-mixing noise primarily concerns jet velocity and pressure relative to ambient airstream velocity and pressure. Details such as noise dissipation from circular ducts are fully addressed through the empirical process. In other cases the noise is calculated at the duct, which leaves us with the task of tackling issues arising from circular duct noise dissipation.

The result of the noise simulation at landing is shown in Fig. 21, for the reference descent slope and for the steep descent at $\gamma = 5.5$ deg. The point $x = 0$ is at touchdown. A simple correction was done to take into account noise attenuation. An average humidity of 50% was considered, and the attenuation rate calculated at the standard atmospheric conditions in the frequency spectrum cut off at 10 kHz. The attenuation depends strongly on the atmospheric humidity and other factors. However, at short distances between

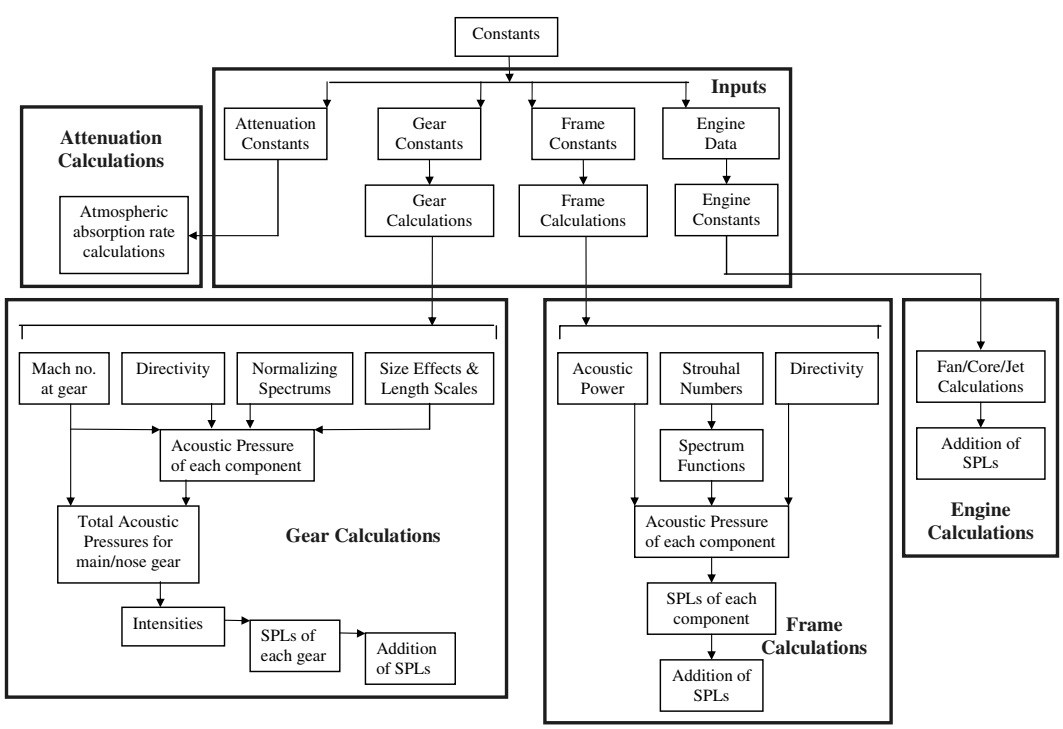

Fig. 20 Flow chart of aircraft noise prediction program.

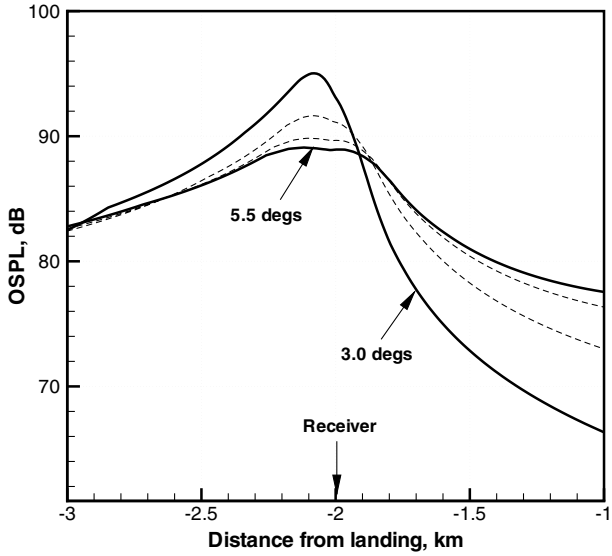

a)

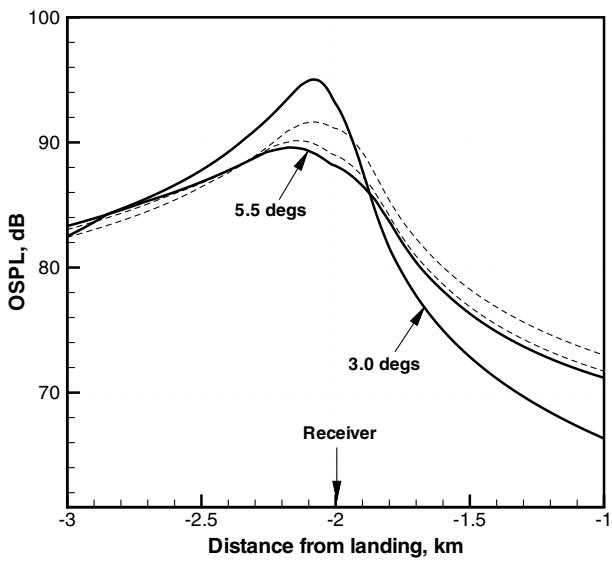

b)

Fig. 21 Calculated OSPL of aircraft model at FAR landing point; $W = 110$ tons.

aircraft and receiver (distances of the order of 200 m), this attenuation is negligible altogether.

The result is striking. In spite of an increase in jet noise (as discussed next), the steep descent cuts the peak overall sound pressure level (OSPL) at the receiver by as much as 6.0 dB. This result is of the same order of magnitude of the estimate provided by Antoine and Kroo [1], although in the latter case the descent angle considered was 4.5 deg, the landing weight was not reported, and the approach speed not discussed.

Further comments are required. First, and foremost, a steep-descent flight path contributes higher noise as the aircraft moves away from the receiver. The main reason for this result is the jet noise, which has increased due to the aircraft *slowing down*. In other words, the jet noise is proportional to V_{rel}^n, with n a high power (equal to 8 in Lighthill's theory). The relative speed between the jet and the aircraft *increases* as the aircraft descends, as a result of the aircraft slowing down for a safe steep descent and the jet speed increasing due to the marginal increase in engine thrust. Another (less dramatic) reason for the change in noise pattern is the change in jet noise directivity.

However, and thankfully, the excessive noise at departure from the receiver can be overcome by changing the flight path. Figure 21 indicates that a flight path with a relax in the terminal descent is a better option in terms of OSPL as the aircraft departs from the receiver.

Table 2 Landing noise at different descent angles; maneuver starts at $h = 457$ m (1500 ft)

γ, deg	OSPL, dB	r, km	X, n mile	t, s	$\bar{T}$, kN
3.0	95.1	0.135	2.78	162.5	135.4
4.0	91.6	0.165	2.29	137.4	136.7
5.0	89.8	0.210	1.86	111.8	136.9
5.5	89.1	0.235	1.69	101.1	137.0

A further analysis of the data has shown that at $\gamma = 5.5$ deg the ratio V/V_{jet} increases by a factor 2 over the flight maneuver, from about 0.12 to 0.24 at the end; in the nominal descent, the range is $V/V_{\mathrm{jet}} = 0.31$–$0.37$. Although flight speed effects have been known for some time (see, for example, Sarohia and Massier [23]), the problem was not completely resolved in this study, and requires further analysis. However, following Lighthill and Ffwocs-Williams [24], the jet noise scales with the relative speed, $V_{\mathrm{rel}} = V_{\mathrm{jet}} - V$.

A parametric analysis was done at the reference descent angles, and the results are summarized in Table 2. The quantity r denotes the distance aircraft-to-receiver at the point of minimum OSPL; X is the ground distance traveled. The aircraft follows the flight path at a constant TAS before stall occurs. Other calculation parameters are: $W = 110$ tons; $p = 1.25$ (e.g., 25% increase in profile drag); $p_1 = 1.025$; $p_2 = 1/1.025$. The result takes into account the Doppler effect.

Consider the case of $\gamma = 5.5$ deg. It is noted that the distance between source and receiver is increased by about 80 m. This corresponds to $r/r_r \simeq 0.74$. In absence of complications such as diffraction, absorption, and reflection, the far-field sound pressure level (SPL) decreases with the distance as $p \propto 1/r^2$. Therefore, by operating the aircraft at $\gamma = 5.5$ deg, the OSPL is expected to decrease by about 45%: all other parameters being the same. This translates into a decrease of OSPL by about 5.5 dB, a figure close enough to the present estimates. In reality the noise reduction is likely to be lower, because of various effects that have been neglected. These effects include variation of airframe noise due to increased C_L and C_D, variation in flap settings, noise attenuation due to actual atmospheric conditions (in particular, relative humidity and frequency bandwidth). However, these approximations must be placed in the context of the overall accuracy of the noise model. Further verification is needed.

VIII. Conclusions

Increasing the descent rate in the terminal area maneuver is of great interest to reducing community noise, to operate short- to medium-range transport aircraft from airfields with limited access, and to increase the volume of traffic at large airports. This paper has addressed some conceptual issues regarding this maneuver. A complete aircraft model with an independent engine simulation and aircraft noise model has been developed and applied.

The main conclusion of this investigation is that the major parameter contributing noise reduction at the measuring station is the larger distance between the aircraft and the receiver. By contrast, the jet noise has to be carefully controlled, because it may yield unwanted results, such as an increase of effective perceived noise (EPNdB), in spite of a decrease in the peak OSPL. This effect may be of great importance in the future operation of aircraft at heavily regulated airports.

The steep descent does not have to be the default mode of landing. In fact, this mode can be avoided whenever geographical constraints and community noise are not critical.

Passenger comfort is not considered critical, because the aircraft follows a straight path as in the nominal case, and decelerates at similar rates. The main concern is passenger awareness that the aircraft is descending too fast, which again justifies the constraint on the terminal descent speed.

The landing gear structural limit does not have to be affected, because the steep maneuver terminates at about 100 m (348 ft) above the runway level. This altitude was considered sufficient to reestablish normal operating procedures and landing as in the conventional approach. Again, the constraint on the terminal descent speed would prevent the aircraft from touching down at a too-high speed.

The change in aerodynamic performance has been investigated. These changes are only notional, because the technology required has not been addressed in detail in the present study. A general conclusion is that an increase in profile drag is required in all possible scenarios. A decrease in lift may also be required to avoid stall.

It was shown that all the methods that increase the profile drag of the aircraft also increase the thrust requirements on the engines. The increase in thrust leads to a modest increase in fuel consumption. The additional thrust (over the reference case) also leads to increased noise emission. However, in the steep-descent flight path the aircraft will be further from the noise receiver's station than in the nominal case, and in most circumstances the overall effect is negligible.

The quantitative conclusions are as follows:

1) A descent at 4 deg is possible without requiring changes in aerodynamics. A descent angle greater than 4 deg cannot be safely achieved by the example aircraft, and possibly by all aircraft in the same category of weight (100–110 tons at landing).

2) A 4-deg descent slope can be coupled with a level flight segment at a higher altitude. This would maintain nearly the same descent pattern as the nominal case, with a reduction in peak OSPL estimated at 3.5 dB.

3) For steeper descent the aerodynamic performance will have to be optimized, so as to increase the $C_{L_{\max}}$ and the $C_D/C_L^{3/2}$ at the same time. The descent factor is important in setting the boundaries for the descent rate; however, the $C_{L_{\max}}$ sets the lower bound for the approach air speed.

4) As the aircraft descends in its high-lift and high-drag configuration, the portion of nonlifting drag decreases; this makes it possible to configure the aircraft to realistically achieve the increase in C_{D_o} required. Calculations have been done with an increase of nonlifting drag up to 33%.

5) The OSPL can be reduced by as much as 6.0 dB with a descent angle of 5.5 deg. However, the noise reduction at departure from the receiver is larger for a steep descent.

6) The maneuver time can be reduced by as much as 60 s, starting from 1000 m (3048 ft). For a 2-min maneuver, this means that the amount of traffic can be increased by 50%.

A wide range of effects has been left out of the analysis and need further consideration. First, we need to address how to recover the aircraft in case of missed approach. The theoretical framework for this study was a standard atmospheric condition, good visibility, and no consideration of externalities such as unavailable runway, head winds, side gusts, or engine failure. Second, the aerodynamic design for high lift must be considered in detail, to improve the descent factor over the whole range of lift coefficients. Third, an investigation is needed into the possible means to increase the nonlifting portion of the drag, without affecting the performance of the high-lift systems. Fourth, an analysis of the overall emissions is required, to avoid an operational handicap on the landing and takeoff emissions (NO_x, CO, HC, soot), as a consequence of operating the aircraft at higher thrust rates.

References

[1] Antoine, N. E., and Kroo, I. M., "Aircraft Optimization for Minimal Environmental Impact," *Journal of Aircraft*, Vol. 41, No. 4, July 2004, pp. 790–797.

[2] Erkelens, L. J. J., "Research on Noise Abatement Procedures," NLR Rept. TP 98066, Amsterdam, 1998.

[3] Erkelens, L. J. J., "Advanced Noise Abatement Procedures for Approach and Departure, AIAA Paper 2002-4858, Aug. 2002.

[4] Clarke, J. P., Ho, N. H., Ren, L., Brown, J. A., Elmer, K. R., Tong, K. O., and Wat, J. W., "Continuous Descent Approach: Design and Flight Test for Lousiville International Airport," *Journal of Aircraft*, Vol. 41, No. 5, Sept. 2004, pp. 1054–1066.

[5] Tong, K., and Warren, A., "Development of Continuous Descent Arrival (CDA) Procedures for Dual-Runway Operations at Houston Intercontinental," AIAA Paper 2006-7750, Sept. 2006.

[6] Visser, W. P. J., and Broomhead, M. J., "GSP: A Generic Object-Oriented Gas Turbine Simulation Environment," ASME Paper 2000-GT-0002, 2000.

[7] Flaig, A., and Hilbig, R., "High Lift Design for Large Civil Aircraft, *High-Lift System Aerodynamics*, CP-515, AGARD, Sept. 1993, pp. 31.1–31.12.

[8] Kiock, R., "The ALVAST Model of DLR," DLR, Technical Rept. IB 129 96/22, Lilienthal Platz, 7, D-38018 Braunschweig, Germany, 1996.

[9] Rudnik, R., Melber, S., Ronzheimer, A., and Brodersen, O., "Three-Dimensional Navier-Stokes Simulations for Transport Aircraft High-Lift Configurations," *Journal of Aircraft*, Vol. 38, No. 5, 2001, pp. 895–903.

[10] Johnson, H. S., and Hagerman, J. R., "Wind-Tunnel Investigation at Low Speed of an Unswept Untapered Semispan Wing of Aspect Ratio 3.13 Equipped with Various 25-Percent-Chord Plain Flaps," NACA Rept. TN 2080, 1950.

[11] Torenbeek, E., *Synthesis of Subsonic Airplane Design*, Kluwer Academic Publishers, Dordrecht, The Netherlands, 1985.

[12] White, F., *Viscous Fluid Flow*, McGraw–Hill, New York, 1974.

[13] Hoerner, S. F., *Fluid Dynamic Drag*, Hoerner Fluid Dynamics, Bakersfield, CA, 1965.

[14] Haftmann, B., Debbeler, F. J., and Gielen, H., "Take-Off Drag Prediction for Airbus A-300-600 and A-310 Compared with Flight Test Results," *Journal of Aircraft*, Vol. 25, No. 12, Nov. 1988, pp. 1088–1096.

[15] Bauer, S. X., "An Aerodynamic Assessment of Micro Drag Generators (MDGs)," AIAA Paper 98-2621, June 1998.

[16] Fink, M. R., "Noise Component Method for Airframe Noise," *Journal of Aircraft*, Vol. 16, No. 10, 1979, pp. 659–665.

[17] Fink, M. R., and Schlinke, R. H., "Airframe Noise Component Interaction Studies," *Journal of Aircraft*, Vol. 17, No. 2, 1980, pp. 99–105.

[18] ESDU, "Airframe Noise Prediction," ESDU International, Data Item 90023, London, June 2003.

[19] Guo, U., "Empirical Prediction of Aircraft Landing Gear Noise," NASA Technical Rept. CR-2005-213780, 2005.

[20] ESDU, "Prediction of Noise Generated by Fans and Compressors in Turbojet and Turbofan Engines," ESDU International, Data Item 98008, London, June 2003.

[21] ESDU, "Estimation of Subsonic Far-Field Jet-Mixing Noise from Single-Stream Circular Nozzles," ESDU International, Data Item 89041, London, Feb. 1990.

[22] ESDU, "Prediction of Combustor Noise from Gas Turbine Engines," ESDU International, Data Item 05001, London, Feb. 2005.

[23] Sarohia, V., and Massier, P. F., "Effects of External Boundary-Layer Flow on Jet Noise in Flight," *AIAA Journal*, Vol. 15, No. 5, May 1977, pp. 659–666.

[24] Ffwocs-Williams, J. E., "The Noise from Turbulence Convected at High Speed," *Philosophical Transactions of the Royal Society of London, Series A: Mathematical and Physical Sciences*, Vol. 255, No. 1061, April 1962, pp. 469–503.